Frontiers in Bioscience Landmark

Front. Biosci. (Landmark Ed) **2026**; 31(1): 47692
https://doi.org/10.31083/FBL47692

Original Research

Unraveling the Interplay of D-2-HG in Glioblastoma Tumorigenesis via Integrated Machine Learning and Molecular Docking Analysis

Yangfan Zou[1,2,†], Xuefei Yu[1,3,†], Qinglin Li[3], Qibiao Wu[1,*], Jing Zhuang[4,*]

[1]Faculty of Chinese Medicine, Macau University of Science and Technology, 999078 Macau, China
[2]Department of Neurosurgery, Zhejiang Cancer Hospital, 310000 Hangzhou, Zhejiang, China
[3]Department of Scientific Research, Zhejiang Cancer Hospital, 310000 Hangzhou, Zhejiang, China
[4]Department of Oncology, Weifang Traditional Chinese Hospital, 261000 Weifang, Shandong, China
*Correspondence: qbwu@must.edu.mo (Qibiao Wu); zhuangjing1226@163.com (Jing Zhuang)
[†]These authors contributed equally.

Academic Editor: Xudong Huang
Submitted: 26 October 2025 Revised: 18 December 2025 Accepted: 24 December 2025 Published: 20 January 2026

Abstract

Background: Glioblastoma (GBM) is an exceptionally aggressive type of brain tumor with a poor prognosis, underscoring the urgent need to identify new molecular targets for therapeutic development. The objective of this research is to clarify the molecular interactions affected by the oncometabolite D-2-hydroxyglutarate (D-2-HG) within the framework of GBM. **Methods**: Differential expression analysis of multi-omics data identified potential target genes linked to GBM pathogenesis. To enhance our understanding of the binding interactions between D-2-HG and the identified target proteins, we utilized an integrated methodology encompassing various machine learning algorithms, network pharmacology techniques, and molecular docking. **Results**: A sum of 135 genes was recognized as possible targets through which D-2-HG exerts its effects in GBM. The ensuing analysis, utilizing machine learning techniques, identified six crucial genes [eukaryotic translation initiation factor 4E binding protein 1 (*EIF4EBP1*), fatty acid binding protein 3 (*FABP3*), potassium voltage-gated channel subfamily Q member 2 (*KCNQ2*), epithelial cell adhesion molecule (*EPCAM*), sphingosine-1-phosphate receptor 5 (*S1PR5*), and metabotropic glutamate receptor 3 (*GRM3*)] as key regulators. Among these, *FABP3*, *KCNQ2*, *EPCAM*, *S1PR5*, and *GRM3* were significantly downregulated, whereas *EIF4EBP1* was markedly upregulated ($p < 0.05$). Molecular docking simulations indicated a strong binding affinity of D-2-HG towards the target proteins. **Conclusions**: Our study suggests that D-2-HG plays a significant role in the pathogenesis of GBM by modulating specific genes and signaling pathways. Utilizing machine learning techniques, we identified six essential regulatory genes, and further molecular docking simulations revealed a strong affinity of D-2-HG for these critical targets. Collectively, these results establish a substantial basis for future investigations into the mechanistic role of D-2-HG in GBM oncogenesis.

Keywords: D-2-hydroxyglutarate (D-2-HG); glioblastoma (GBM); key genes; machine learning; molecular docking

1. Introduction

Glioblastoma (GBM) represents the most prevalent and aggressive type of primary malignant brain tumor found in adults. It is distinguished by its rapid growth, resistance to standard treatment modalities, and poses a significant risk to both the survival and quality of life of affected individuals [1]. Presently utilized therapeutic strategies, such as surgical intervention, radiotherapy, chemotherapy, and tumor-treating fields, demonstrate restricted effectiveness owing to significant tumor heterogeneity and the presence of the blood-brain barrier, which obstructs the delivery of pharmacological agents, while research on the core molecular mechanisms driving GBM progression faces significant challenges [2–4]. In the past few years, there have been notable developments in the field of molecular pathology, especially regarding the identification of mutations in isocitrate dehydrogenase (*IDH*) and the associated oncometabolite D-2-hydroxyglutarate (D-2-HG), have brought hope for elucidating the core mechanisms underlying GBM pathogenesis and development [5,6]. IDH plays a vital role as an enzyme in the tricarboxylic acid (TCA) cycle, where it is chiefly tasked with promoting the oxidative decarboxylation of isocitrate, resulting in the formation of alpha-ketoglutarate (α-KG). Notably, mutations in *IDH* are observed in more than 80% of gliomas, specific point mutations occur in the *IDH1* or *IDH2* genes, such as *IDH1* Arginine 132 (Arg132) or *IDH2* Arginine 172 (Arg172) [7,8]. The mutant IDH assumes a "neomorphic" role, facilitating the conversion of α-KG into substantial quantities of D-2-HG, which abnormally accumulates within cellular environments, often achieving millimolar levels. The elevated concentrations of D-2-HG serve as competitive inhibitors for a range of α-KG-dependent dioxygenases, with particular emphasis on histone demethylases such as jumonji domain containing 2A (JMJD2A) and jumonji domain containing 2C (JMJD2C), as well as members of the ten-eleven translocation (TET) family of DNA demethylases. This inhibition triggers a widespread hypermethylation of both histones and DNA across the genome, culminating in the emer-

Copyright: © 2026 The Author(s). Published by IMR Press.
This is an open access article under the CC BY 4.0 license.

Publisher's Note: IMR Press stays neutral with regard to jurisdictional claims in published maps and institutional affiliations.

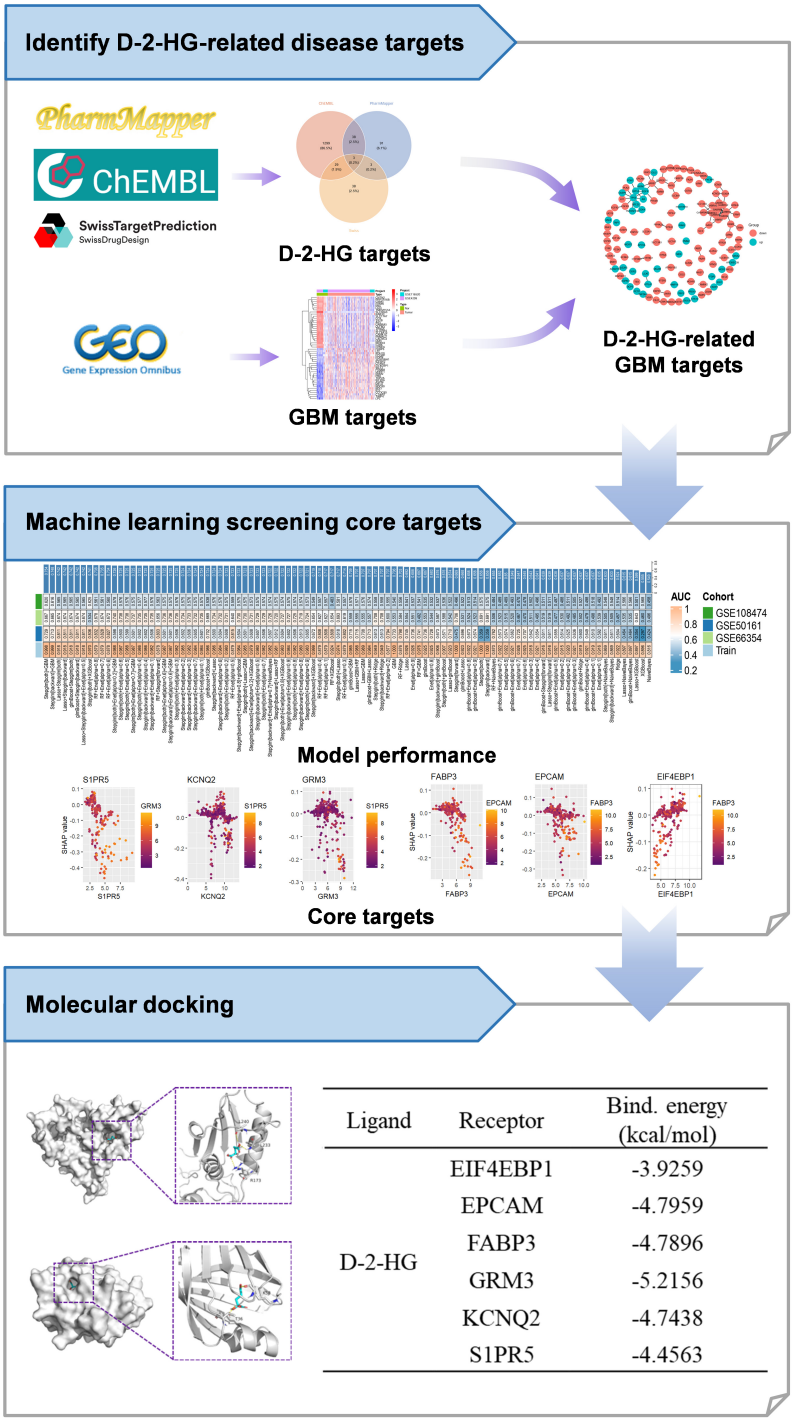

Ligand	Receptor	Bind. energy (kcal/mol)
D-2-HG	EIF4EBP1	-3.9259
	EPCAM	-4.7959
	FABP3	-4.7896
	GRM3	-5.2156
	KCNQ2	-4.7438
	S1PR5	-4.4563

Fig. 1. The analytical workflow employed for the datasets in the study. D-2-HG, D-2-hydroxyglutarate; GBM, glioblastoma; EIF4EBP1, eukaryotic translation initiation factor 4E binding protein 1; EPCAM, epithelial cell adhesion molecule; FABP3, fatty acid binding protein 3; GRM3, metabotropic glutamate receptor 3; KCNQ2, potassium voltage-gated channel subfamily Q member 2; S1PR5, sphingosine-1-phosphate receptor 5.

gence of a unique "glioma CpG island methylator phenotype" (G-CIMP). This epigenetic alteration silences tumor suppressor genes such as cyclin dependent kinase inhibitor 2A (CDKN2A), while aberrantly activating oncogenes like platelet derived growth factor receptor alpha (PDGFRA) through methylation-dependent regulation, ultimately causing cell differentiation arrest and uncontrolled proliferation, thereby promoting gliomagenesis [9–11]. Furthermore, D-2-HG can induce hypermethylation of promoter regions of interferon signaling-related genes [e.g., interferon regula-

tory factor 1 (IRF1), signal transducer and activator of transcription 1 (STAT1)], thereby suppressing anti-tumor immune responses.

The importance of the oncometabolite D-2-HG seems to be intricately nuanced and may exhibit dual characteristics depending on the context [12]. A notable clinical contradiction exists whereby gliomas harboring *IDH* mutations, which are marked by the accumulation of D-2-HG, exhibit a considerably improved prognosis. Specifically, the median overall survival for patients with these mutations is reported to be 3.8 years, in contrast to just 1.1 years for those with the wildtype variant. Furthermore, these *IDH*-mutant gliomas demonstrate heightened responsiveness to temozolomide (TMZ) treatment [13]. At the molecular level, studies suggest that D-2-HG can exert tumor-suppressive effects in certain contexts, for instance, by downregulating the integrin subunit beta 4 (ITGB4)/phosphatidylinositol 3-kinase (PI3K)/Akt serine/threonine kinase (AKT) signaling axis, thereby inhibiting proliferation and promoting apoptosis. This function contrasts sharply with its known oncogenic activity of inhibiting α-KG-dependent dioxygenases and inducing epigenetic silencing, underscoring a dose-, time-, or tissue-dependent duality in its mechanism of action [14]. Research indicates that D-2-HG inhibits the RNA demethylase fat mass and obesity-associated protein (FTO), leading to elevated levels of N6-methyladenosine (m6A) modifications on mRNA transcripts, such as activating transcription factor 5 (ATF5) and MYC Proto-Oncogene, BHLH Transcription Factor (MYC). This consequently reduces the stability of these oncogenic transcripts, providing an explanation for the restricted growth observed in *IDH*-mutant tumors [15]. Despite considerable advancements in this field, current research efforts remain predominantly confined to single-omics approaches, emphasizing linear signaling pathways rather than systems-level network effects. To address this gap, our study focuses on reconstructing the molecular network linking D-2-HG to GBM pathogenesis through integrative multi-omics analysis. We utilize machine learning-based analyses of topological and functional enrichment to identify key hub molecules within the network. This is subsequently complemented by molecular docking simulations to assess target binding affinity and the thermodynamics of interactions. Through this approach, we aim to clarify the complex regulatory network governed by D-2-HG, this work aims to identify key drivers of GBM oncogenesis and progression, potentially revealing novel therapeutic targets to overcome current treatment limitations.

2. Materials and Methods

2.1 Acquisition of Key Genes in GBM

Transcriptome datasets sourced from five GBM studies, namely GSE4290, GSE116520, GSE66354, GSE50161, and GSE108474, were obtained from the National Center for Biotechnology Information (NCBI, https://www.ncbi.nlm.nih.gov/) Gene Expression Omnibus (GEO) repository. The datasets GSE4290 and GSE116520 were classified as the discovery cohort, whereas the other three datasets (GSE66354, GSE50161, GSE108474) functioned as independent validation cohorts. To address potential batch effects, a comprehensive normalization pipeline was employed: the initial step involved the application of Surrogate Variable Analysis (SVA) utilizing the svaR package (version 3.46.0 1), aimed at modeling and correcting for latent confounding factors present within the discovery cohort [16]. Following this, ComBat harmonization was utilized within a parametric empirical Bayes framework to address and adjust for any remaining batch effects [17]. The effectiveness of the integrated data was assessed using principal component analysis (PCA), which demonstrated improved clustering of inter-batch samples within a lower-dimensional space, thus affirming the successful harmonization of the data. A detailed representation of the analytical workflow is illustrated in Fig. 1.

2.2 Acquisition of D-2-HG Chemical Properties and Key Targets

The chemical characterization of D-2-HG was achieved through the integration of information from multiple databases. The pertinent physicochemical characteristics and biological metrics were methodically gathered from PubMed, whereas the standard two-dimensional structural molecular formula (SMILES: C(CC(=O)O)C(C(=O)O)O) was sourced from the PubChem database. Target prediction for this molecule was conducted utilizing three specialized databases: the ChEMBL Database, which was used for profiling ligand-receptor interactions; Swiss Target Prediction, applied for chemogenomics-based target identification (http://www.swisstargetprediction.ch); and Reverse Pharmacophore Mapping, executed via three-dimensional pharmacophore matching utilizing the Pharm Mapper platform (https://lilab-ecust.cn/pharmmapper/index.html). All identified targets were limited to the human proteome to maintain biological relevance.

2.3 Differential Gene Expression Analysis

The evaluation was conducted utilizing the limma package (version 3.62.2) within the R programming environment, which incorporates a linear modeling framework along with empirical Bayes moderation to analyze differential expression on a transcriptome-wide level. Genes were categorized as statistically significantly differentially expressed genes (DEGs) when they demonstrated a false discovery rate (FDR)-adjusted p-value of less than 0.05, in addition to an absolute log2 fold change greater than 0.585, which equates to a 1.5-fold change. The outcomes of the analysis, which included the distribution of DEGs, were illustrated through the ggplot2 visualization system, facili-

tating the creation of high-quality figures appropriate for publication, such as volcano plots.

2.4 Weighted Gene Co-Expression Network Analysis (WGCNA)

The analysis pipeline included: sample quality control via hierarchical clustering to remove outliers; establishing an ideal soft-thresholding power guided by the principles of scale-free topology (R^2 >0.85); the identification of modules was conducted through hierarchical clustering applied to a topological overlap matrix (TOM), utilizing a minimum module size threshold of 30. Additionally, a merge cut height of 0.25 was implemented to refine the clustering results. Subsequently, an analysis of the association between the identified modules and various traits was performed by correlating module eigengenes with phenotypes (|Pearson's r| >0.5, $p < 0.05$); and the determination of essential genes through the analysis of significant intramodular connectivity (kME >0.8).

2.5 Identification of D-2-HG-Related Targets

This involved taking the intersection of genes highlighted as significant through DEGs and WGCNA with the set of genes predicted to be targets of D-2-HG. The outcome of this targeted filtering was graphically summarized with a Venn diagram to delineate the overlapping gene set.

2.6 Functional Enrichment Analysis

To investigate the involvement of D-2-HG in the development of GBM, Gene Ontology (GO) analyses encompassing Biological Process (BP), Cellular Component (CC), and Molecular Function (MF), along with Kyoto Encyclopedia of Genes and Genomes (KEGG, https://www.kegg.jp/) pathway analyses, were conducted utilizing the clusterProfiler package (version 4.16.0), with a significance threshold set at $p < 0.05$.

2.7 Core Gene Selection Based on Machine Learning

We utilize machine learning-based analyses of topological and functional enrichment to identify key hub molecules within the network. This is subsequently complemented by molecular docking simulations to assess target binding affinity and the thermodynamics of interactions. Through this approach, we aim to clarify the complex regulatory network governed by D-2-HG [18], to develop a total of 98 predictive models. Hyperparameter optimization was conducted utilizing cross-validation techniques, and stratified sampling was employed to divide seven distinct datasets into training and internal validation subsets. The efficacy of the models was thoroughly evaluated using a range of metrics, among which was the area under the receiver operating characteristic (ROC) curve (AUC), overall accuracy, and the F1-score. Following this, a Stacking ensemble learning approach was implemented to amalgamate the predictions derived from the most effective individual models. Models demonstrating high confidence, defined as having an AUC greater than 0.7, were selected, and their associated feature genes were ranked based on their frequency to pinpoint potential core genes. Ultimately, the gene expression patterns were visualized utilizing the pheatmap package (version 1.0.13).

2.8 Model Analysis

Given the inherently opaque nature of machine learning algorithms, we utilized the SHAP (SHapley Additive exPlanations) approach to assess the impact of specific features on the predicted results. This method determines a SHAP value for each feature, facilitating a clear understanding of its role in the predictions made by the model.

2.9 Molecular Docking Analysis

Computational validation of the binding interactions between the oncometabolite D-2-HG and the prioritized core genes was carried out through molecular docking simulations. The initial 3D coordinates of the D-2-HG ligand were acquired in Structure Data File (SDF) format from PubChem [19]. The three-dimensional structures of the corresponding target proteins were downloaded from the UniProt database. Critical pre-docking preparations included preprocessing the protein structures to remove crystallographic water molecules and define the protonation state by adding hydrogen atoms. The ligand structure was similarly subjected to geometry optimization using the Merck Molecular Force Field (MMFF) to ensure an energetically favorable conformation. For each target, the docking grid box was strategically centered on the predicted active site, with its size parameters meticulously adjusted to accommodate the ligand's dimensions and allow for comprehensive exploration of potential binding poses [20]. All docking calculations were executed using the Molecular Operating Environment (MOE) software (MOE 2019.0102) suite (Montreal, Quebec, Canada). The output docking poses were subsequently imported into PyMOL for detailed structural analysis, visualization, and generation of publication-quality figures.

3. Results

3.1 Identification of D-2-HG Target Protein

The molecular configuration of D-2-HG was obtained from the PubChem database, as illustrated in Fig. 2A. A comprehensive analysis to predict potential biological targets for D-2-HG was performed utilizing three complementary databases: ChEMBL, which catalogs annotated bioactive molecules, reverse pharmacophore mapping, additionally, Swiss Target Prediction is utilized, emphasizing ligand-centric target forecasting. Following the integration of the data and the removal of redundant entries, a unified collection comprising 1501 potential targets was created (Fig. 2B).

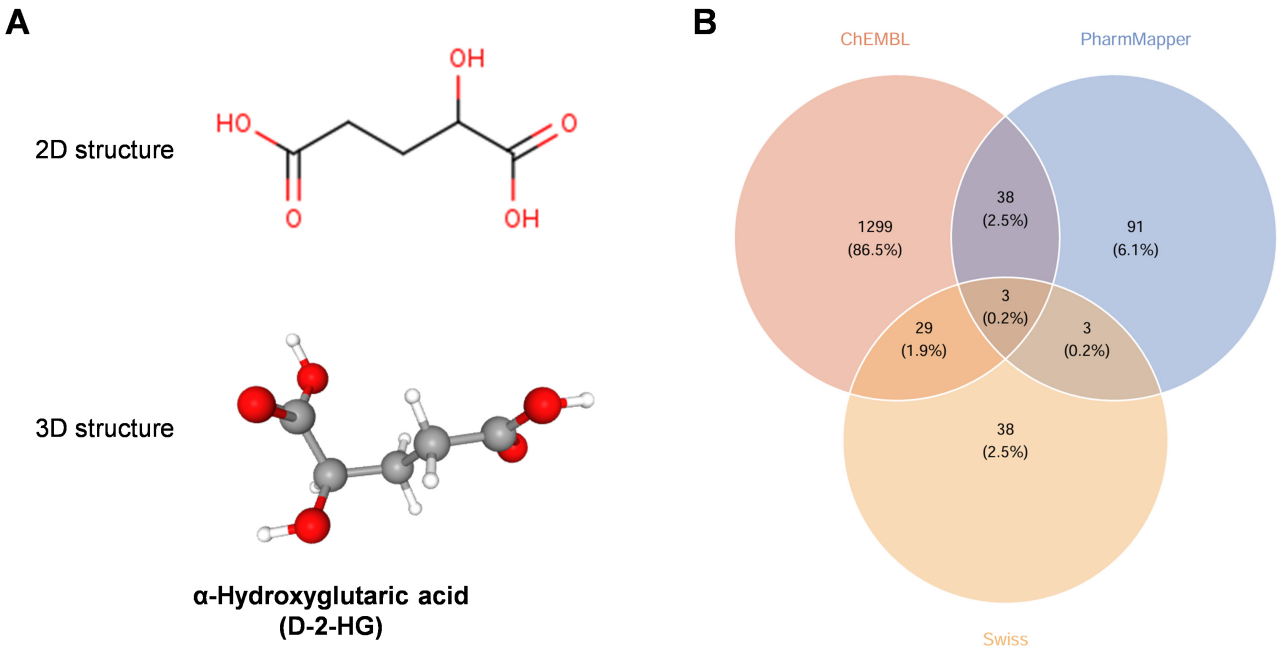

Fig. 2. Identification of target proteins for D-2-HG. (A) The chemical structure (2D & 3D) of D-2-HG. (B) The prediction of potential targets was conducted utilizing ChEMBL, PharmMapper, and SwissTargetPrediction methodologies.

3.2 Identification of Target Genes Associated With GBM

In order to address batch effects, datasets GSE4290 and GSE116520 were combined and underwent thorough normalization of the gene expression matrix. The implementation of PCA demonstrated an improved data distribution subsequent to normalization, with the normalized dataset exhibiting more distinct clustering patterns (Fig. 3A,B). The differential expression analysis identified 2017 genes that displayed significant alterations in GBM. These changes in expression were depicted using both a heatmap and a volcano plot (Fig. 3C,D). In the context of WGCNA, the ideal soft-thresholding power (β) was initially determined to construct a scale-free network topology. A comprehensive evaluation of power values ranging from 1 to 20 revealed that a β value of 3 constituted the minimal threshold necessary to satisfy the criteria for scale-free topology ($R^2 \geq 0.8$). By employing this parameter, a TOM was created, which was subsequently followed by hierarchical clustering to identify co-expression modules. This analysis culminated in the discovery of eight distinct gene modules, each distinguished by a specific color for enhanced clarity (Fig. 3E). The module-trait relationship analysis uncovered significant correlations ($p < 0.05$) between certain modules and GBM (Fig. 3F). By combining DEGs from the traditional analysis with genes from WGCNA (after eliminating duplicates), the intersection of these two groups was established, leading to a final compilation of 1563 genes associated with GBM (Fig. 3G).

3.3 Identification of D-2-HG Related Targets in GBM

The intersection analysis between D-2-HG-associated genes and GBM-related genes identified 135 overlapping genes involved in the potential molecular mechanism (Fig. 4A). The interaction network of these common targets was visualized, distinguishing between upregulated and downregulated genes (Fig. 4B). Functional characterization through GO and KEGG enrichment analyses (Fig. 4C,D) revealed comprehensive molecular insights. GO analysis demonstrated significant enrichment in gamma-aminobutyric acid (GABA) signaling pathways and regulation of membrane potential (BPs), ion channel complexes and synaptic membranes (CCs), as well as GABA receptor activity and gated channel activity (MFs). KEGG pathway analysis highlighted crucial involvement in growth factor signaling (GF-RTK-RAS-ERK), signaling cascades [PI3K, protein 53 (P53)], and cell cycle regulation (G1/S transition). These findings collectively indicate significant modulation of neurotransmitter signaling, activation of oncogenic pathways, and cell cycle dysregulation in the context of D-2-HG and GBM interaction.

3.4 Identification of Core Genes Involved in the Regulation of GBM by D-2-HG

To decode the core genes associated with D-2-HG-related GBM, we performed a comprehensive machine learning analysis on 135 candidate targets, constructing a total of 98 predictive models. Among these, the Stepglm [both] + GBM ensemble model outperformed others, yielding the highest accuracy across both training and validation cohorts (Fig. 5A). This computational pipeline iden-

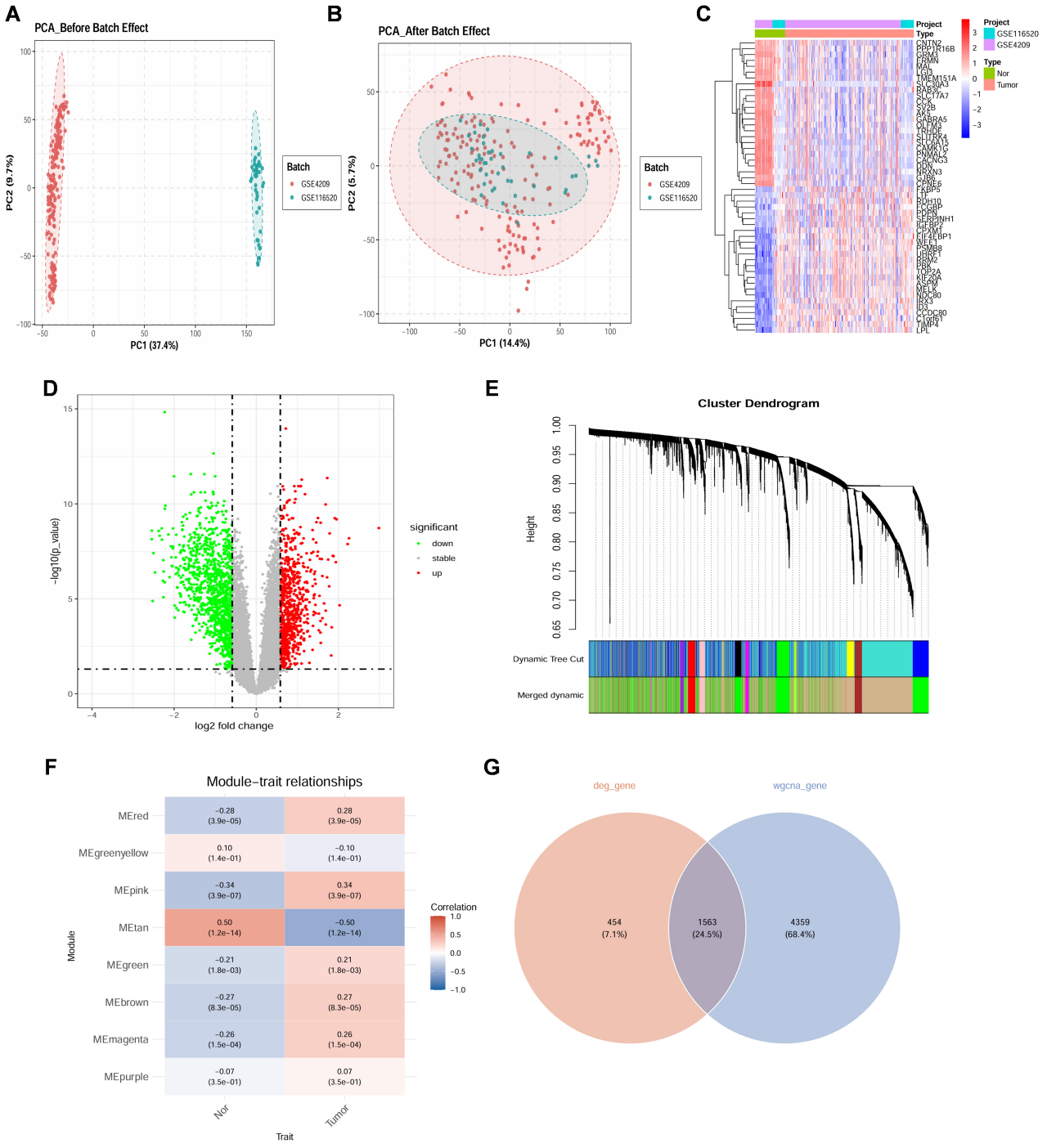

Fig. 3. Identification of Target genes associated with GBM. (A) The principal component analysis (PCA) scatter plot illustrates a clear distinction between the GSE4290 and GSE116520 datasets prior to the implementation of batch correction, signifying the presence of batch effects. (B) Following batch correction, the PCA scatter plot demonstrates the successful integration of the GSE4290 and GSE116520 datasets, reflecting a significant reduction in batch effects. (C) The heatmap presents the expression patterns of differentially expressed genes (DEGs) across the samples, where red denotes upregulation and blue signifies downregulation. (D) The volcano plot visualizes the DEGs in relation to log2 fold change (log2FC) and statistical significance, with red dots representing upregulated genes, green dots indicating downregulated genes, and grey dots denoting genes that are not statistically significant. (E) Gene dendrogram from weighted gene co-expression network analysis (WGCNA) shows hierarchical clustering based on co-expression. Module colors in the lower panel represent different gene modules. (F) Module-trait relationships heatmap shows correlations between WGCNA-identified modules and sample traits (Control vs. Treatment). Values in boxes indicate correlation coefficients and *p*-values. (G) Venn diagram shows DEGs (red) and WGCNA modules (blue), with purple indicating common genes from both methods.

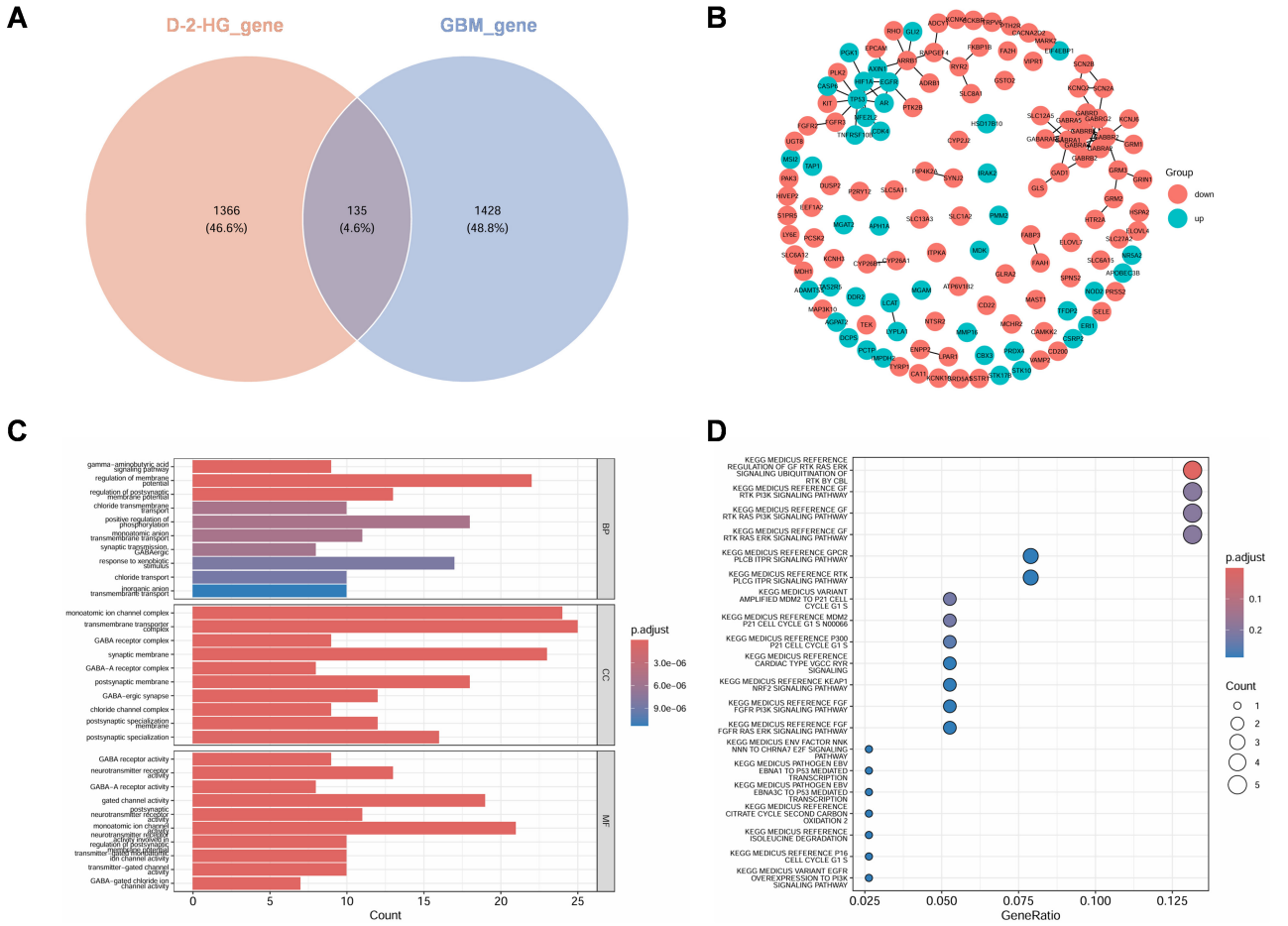

Fig. 4. Identification of disease targets associated with D-2-HG in GBM. (A) A Venn diagram illustrates the comparison between genes associated with D-2-HG exposure (depicted in red) and those related to GBM (represented in blue), revealing a total of 135 genes that are common to both categories, accounting for 4.6% of the total. (B) The Protein-Protein Interaction (PPI) network delineates the relationships among these overlapping genes, where red nodes indicate upregulated genes, green nodes signify downregulated genes, and the edges represent predicted interactions. (C) Gene Ontology (GO) enrichment analysis categorizes the overlapping genes into Biological Process (BP), Cellular Component (CC), and Molecular Function (MF). The X-axis denotes the gene count, while the color gradient reflects the adjusted *p*-value, with darker red shades indicating greater significance. (D) The Kyoto Encyclopedia of Genes and Genomes (KEGG) analysis highlights the pathways that are enriched for the overlapping genes. The X-axis illustrates the gene ratio, the size of the dots corresponds to the gene count, and the color gradient indicates the adjusted *p*-value, with red representing higher significance.

tified a signature of six pivotal genes: eukaryotic translation initiation factor 4E binding protein 1 (*EIF4EBP1*), fatty acid binding protein 3 (*FABP3*), potassium voltage-gated channel subfamily Q member 2 (*KCNQ2*), epithelial cell adhesion molecule (*EPCAM*), sphingosine-1-phosphate receptor 5 (*S1PR5*), and metabotropic glutamate receptor 3 (*GRM3*). The diagnostic robustness of these hubs was corroborated by ROC curve analysis (AUC >0.70, Fig. 5B), while their distinct expression profiles in GBM tissues were visualized via volcano plots (Fig. 5C). SHAP analysis was subsequently employed to quantify functional contributions, highlighting *S1PR5* (SHAP value = 0.0622) and *KCNQ2* (0.0438) as the most influential predictors (Fig. 5D). Interestingly, the SHAP values for most genes were predominantly negative, suggesting that these targets may exert an inhibitory effect on the model's predictive output following D-2-HG intervention. In contrast, *EIF4EBP1* emerged as the sole definitive oncogene; although its SHAP values fluctuated, high expression levels consistently trended toward positive values, underscoring its pro-tumorigenic role (Fig. 5E). Further analysis of individual gene interactions revealed that low expression of *S1PR5* (<5) was associated with dispersed but generally low SHAP values (approximately –0.3 to 0.0), indicating a stronger tumor-suppressive effect when its expression is lost. This supports the hypothesis that *S1PR5*

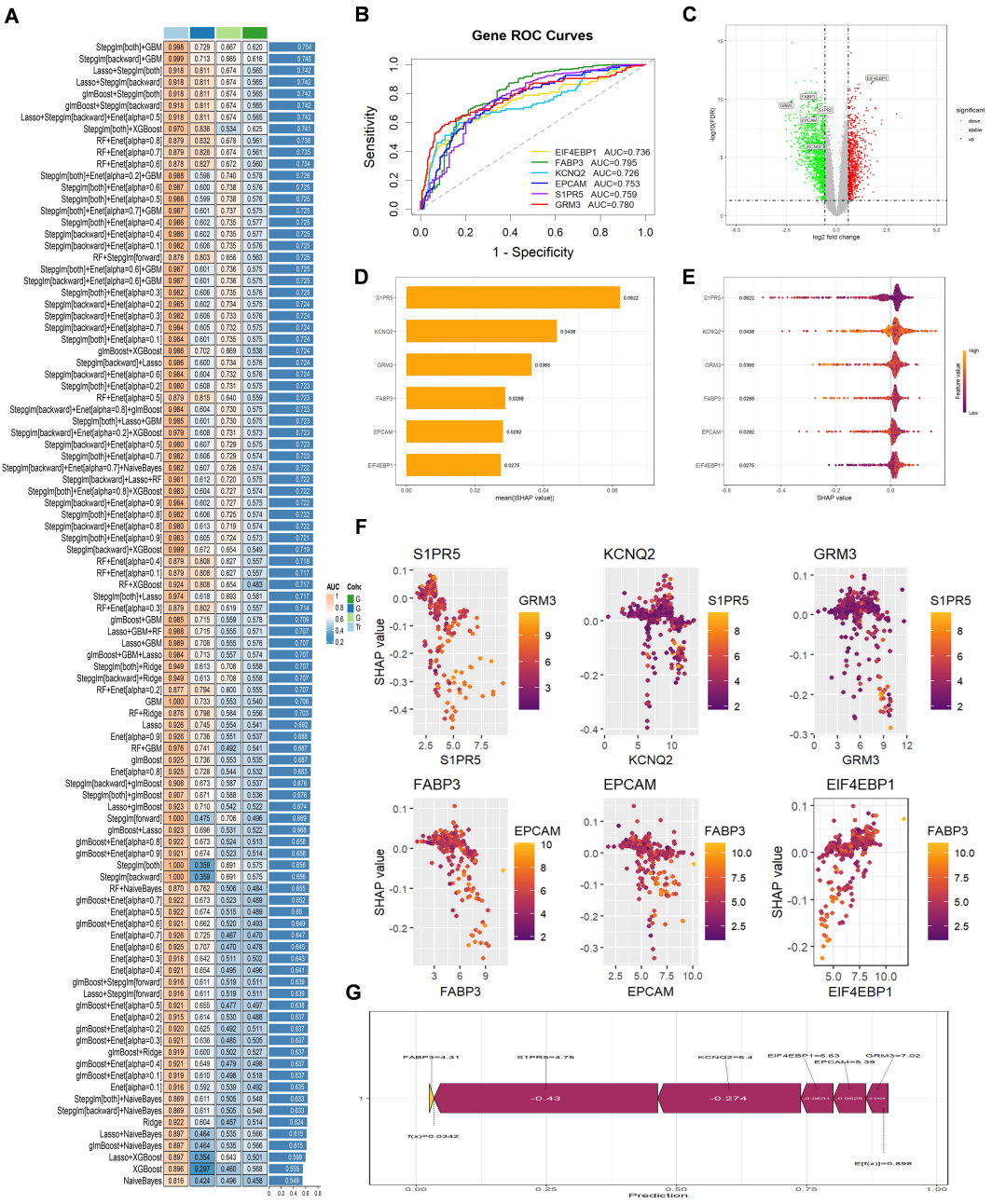

Fig. 5. Identification of essential genes involved in D-2-HG-induced GBM. (A) Comparative Analysis of Model Performance: The heatmap illustrates the area under the curve (AUC) values for different models across various cohorts. The left column represents the models, while the right column displays the corresponding AUC values (with higher values indicating superior performance). The color coding reflects the sources of the cohorts. (B) ROC Curves: ROC curves for key genes (*EIF4EBP1*, *FABP3*, *KCNQ2*, *EPCAM*, *S1PR5*, *GRM3*). X-axis = false positive rate, Y-axis = sensitivity. AUC indicates predictive performance. (C) Volcano Plot: volcano plot shows DEGs. X-axis = log2FC, Y-axis = –log10(*p*-value). Red = upregulated, green = downregulated, with key genes labeled. (D) Feature Importance Ranking: A bar graph ranks top genes by feature importance. Larger bars = greater contribution to the model. (E) Violin Plot: violin plot shows gene expression distributions across conditions. Width represents data density, while colors indicate expression levels. (F) SHAP (SHapley Additive exPlanations) Value Distribution: The scatter plots illustrate the distribution of SHAP values for significant genes, highlighting their influence on predictive outcomes. (G) SHAP Summary Plot: The summary plot of SHAP values reveals the contributions of various genes to the predictions. A negative SHAP value signifies a diminishing effect, whereas a positive value indicates an enhancing effect.

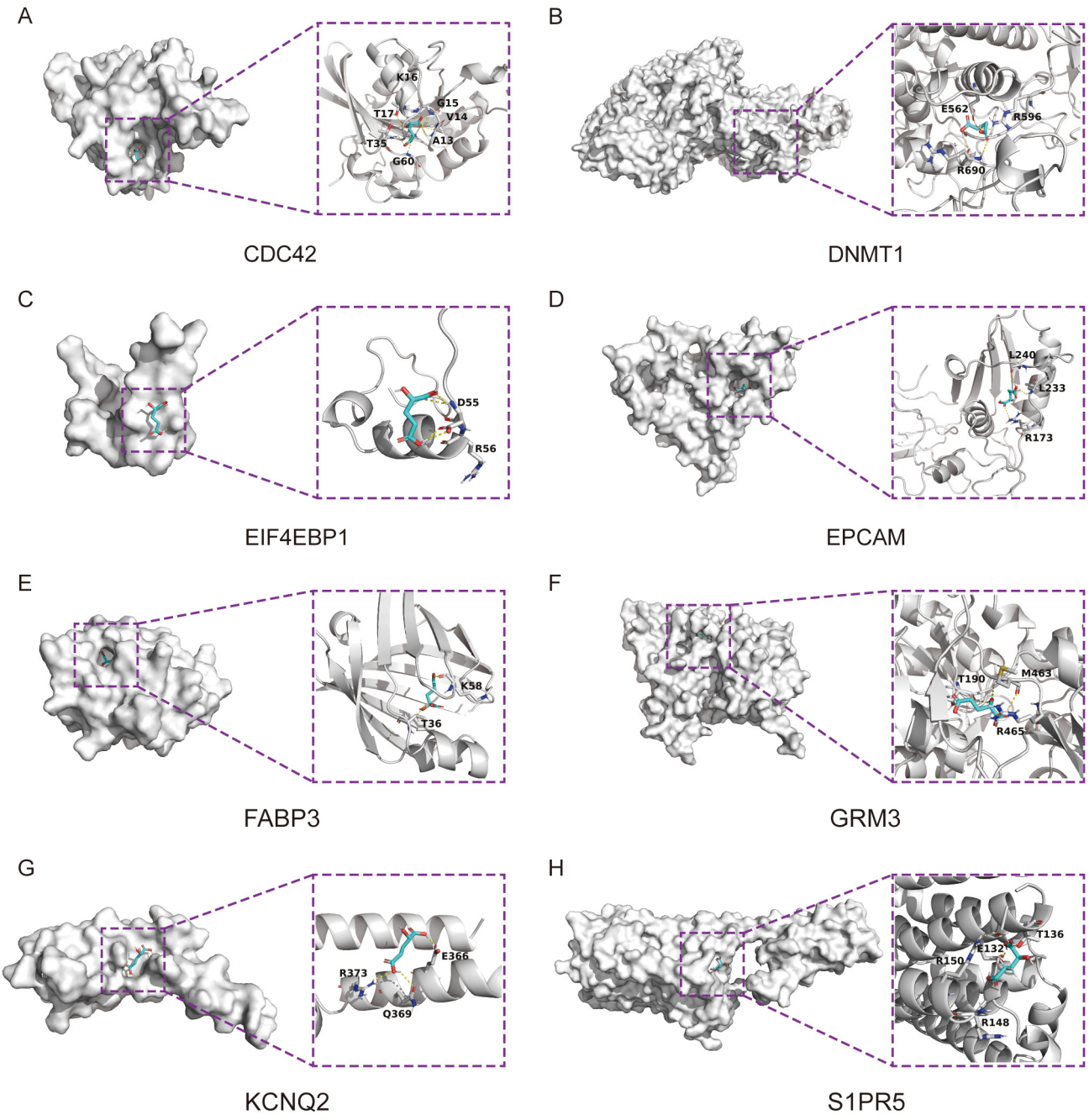

Fig. 6. Validation of molecular docking for D-2-HG-Core gene interactions. (A) Docking analysis of CDC42 with D-2-HG. (B) Docking analysis of DNMT1 in association with D-2-HG. (C) Docking analysis of EIF4EBP1 in association with D-2-HG. (D) Docking analysis of EPCAM in relation to D-2-HG. (E) Docking analysis of FABP3 in connection with D-2-HG. (F) Docking analysis of GRM3 in conjunction with D-2-HG. (G) Docking analysis of KCNQ2 with D-2-HG. (H) Docking analysis of S1PR5 in association with D-2-HG.

may be indirectly regulated by D-2-HG, with its downregulation potentially driving tumor progression. Notably, even when *GRM3* was highly expressed (warm-colored points), the SHAP values for *S1PR5* remained concentrated in the negative region (–0.1 to –0.4), suggesting possible co-expression patterns (e.g., simultaneous downregulation) but providing no evidence for direct regulatory control of *S1PR5* by *GRM3* in the oncogenic process. A noticeable shift in SHAP values for *S1PR5* (from –0.3 to –0.1) was observed at an expression level around 4–5, potentially indicating a biological threshold (such as a pathway activation critical point). This implies that *S1PR5* expression may need to fall below a specific threshold to significantly exert its tumor-suppressive function, providing a rationale for subsequent mechanistic studies (e.g., gene silencing) (Fig. 5F). Overall, S1PR5 and *KCNQ2* were identified as the primary contributors (largest absolute SHAP values), whose expression effectively reduced tumor risk (Fig. 5G).

Table 1. Binding ability of ligands and receptors.

Ligand	Receptor	Bind. energy (kcal/mol)	Bind. sites
D-2-HG	CDC42	–5.2580	A13, V14, G15, K16, T17, T35, G60
	DNMT1	–4.9684	E562, R596, R690
	EIF4EBP1	–3.9259	D55, R56
	EPCAM	–4.7959	L173, L233, L240
	FABP3	–4.7896	T36, K58
	GRM3	–5.2156	T190, M463, R465
	KCNQ2	–4.7438	E366, Q369, R373
	S1PR5	–4.4563	E132, T136, R148, R150

CDC42, cell division cycle 42; DNMT1, DNA methyltransferase 1.

3.5 Molecular Docking Verification of the Interaction Between D-2-HG and Core Genes

To assess the possible binding interactions of D-2-HG with the protein products of the identified core genes (*EIF4EBP1*, *FABP3*, *KCNQ2*, *EPCAM*, *S1PR5*, *GRM3*), a detailed molecular docking analysis was conducted. To validate the reliability of our docking protocol and establish a comparative baseline, we additionally performed docking simulations between D-2-HG and two reference proteins: cell division cycle 42 (CDC42) and DNA methyltransferase 1 (DNMT1) [21,22]. The results indicated that D-2-HG exhibited a notable binding affinity across all six identified target proteins, with binding energies comparable to or exceeding those of the reference controls (CDC42: [–5.2580] kcal/mol; DNMT1: [–4.9684] kcal/mol). This implies the formation of stable and spontaneous molecular complexes. In accordance with the established criteria in molecular docking studies, a binding energy threshold of less than 0 kcal/mol signifies spontaneous binding, while values falling below –5.0 kcal/mol reflect an exceptional binding affinity (see Table 1). The visualization of the binding conformations, as depicted in Fig. 6, further corroborated the stability of the docking arrangements for all D-2-HG–protein complexes. These findings provide structural evidence that underpins the direct molecular interactions between D-2-HG and the GBM-related core targets identified via our machine learning approach.

4. Discussion

The oncogenic effects of D-2-HG in GBM primarily stem from gain-of-function mutations in the *IDH* gene, particularly the *IDH1 R132H* mutation [23,24]. This mutation confers a neomorphic activity upon *IDH1*, enabling it to excessively reduce the normal TCA cycle metabolite α-KG into D-2-HG, leading to its abnormal accumulation within tumor cells, with concentrations reaching millimolar levels [25]. D-2-HG competitively inhibits a range of α-KG-dependent dioxygenases, thereby inducing widespread epigenetic dysregulation [26]. The core oncogenic mechanism involves the potent inhibition of TET family DNA demethylases and histone demethylases [e.g., lysine demethylase (KDM) family] by D-2-HG. This silences numerous genes associated with cell differentiation and tumor suppression are silenced, trapping glioma cells in an undifferentiated, proliferative state [10]. Furthermore, D-2-HG can inhibit prolyl hydroxylases (PHDs), stabilizing hypoxia-inducible factor HIF-1α, which promotes tumor angiogenesis, glycolysis, and adaptation to the hypoxic microenvironment [27,28]. Notably, the oncogenic action of D-2-HG involves significant synergistic enhancing factors and is closely linked to the activity states of specific epigenetic regulators [29]. For instance, in *IDH*-wildtype GBM, arginine methyltransferase protein arginine methyltransferase 1 (PRMT1) is recruited to 5hmC-enriched regions to catalyze activating histone marks. However, in the *IDH*-mutant context, D-2-HG accumulation may inhibit protein arginine methyltransferase 5 (PRMT5) function, leading to a relative dominance of PRMT1 activity, which can drive alternative oncogenic pathways, illustrating the plasticity of tumor epigenetic regulation [30]. Beyond direct epigenetic regulation, D-2-HG promotes GBM progression through other pathways, with its role in shaping the tumor immune microenvironment being particularly important [31,32]. D-2-HG secreted by tumor cells can be taken up by CD8+ T cells in the microenvironment. It directly inhibits the activity of lactate dehydrogenase (LDH), disrupting the glycolytic process in CD8+ T cells [33,34]. This metabolic disruption impairs T cell proliferation and cytokine production [e.g., interferon gamma (IFN-γ)], ultimately facilitating tumor immune escape [35].

A comprehensive analysis of multi-omics data, utilizing sophisticated machine learning techniques alongside bioinformatics methodologies, has systematically revealed potential molecular targets that connect D-2-HG to the development of GBM. Through a rigorous screening process, six core genes—*EIF4EBP1*, *FABP3*, *KCNQ2*, *EPCAM*, *S1PR5*, and *GRM3*—were found to be particularly prominent. Differential expression analysis revealed that *EIF4EBP1* was upregulated in GBM, while *FABP3*, *KCNQ2*, *EPCAM*, *S1PR5*, and *GRM3* were downregulated. The application of machine learning models has substantiated the significant diagnostic potential of the identified gene signature. Interpretative analysis utilizing SHAP values revealed that *S1PR5* (SHAP value = 0.0622) and

KCNQ2 (SHAP value = 0.0438) emerged as the most pivotal predictors. Furthermore, molecular docking simulations provided additional evidence for the biological implications of these results, demonstrating a robust binding affinity between D-2-HG and the products of the core genes, facilitated by specific interactions among amino acids.

The identified core genes exert their functions through a cross-regulatory axis involving metabolism, epigenetics, and signaling pathways, and may exhibit significant synergistic or antagonistic interactions with the oncogenic metabolite D-2-HG produced by *IDH* mutation. D-2-HG, which accumulates due to *IDH* mutations, can competitively inhibit α-KG-dependent dioxygenases, leading to epigenetic dysregulation such as DNA hypermethylation, which may interact with the functions of these core genes [14]. EIF4EBP1 (Eukaryotic Translation Initiation Factor 4E-Binding Protein 1) serves as a pivotal effector within the mTOR signaling pathway. In the context of glioma, its function extends beyond mere translational repression, exhibiting a tight coupling with the metabolic microenvironment. Functioning primarily as a negative regulator of mRNA translation, EIF4EBP1 acts as a direct substrate of mTOR and inhibits the assembly of the translation initiation complex by sequestering eIF4E [36]. Investigations reveal a dual regulatory mechanism for EIF4EBP1 in *IDH*-mutant gliomas. On one hand, D-2-HG accumulation precipitates metabolic stress ("energy crisis"), activating adenosine monophosphate-activated protein kinase (AMPK). Activated AMPK suppresses mechanistic target of rapamycin complex 1 (mTORC1), keeping EIF4EBP1 hypophosphorylated. This drives "translational reprogramming" to prioritize stress-response proteins, conferring a survival advantage in harsh environments. On the other hand, EIF4EBP1 overexpression correlates with tumor aggressiveness and is frequently observed in GBM [37]. This upregulation is driven by oncogenic transcription factors like MYB proto-oncogene like 2 (MYBL2) and Transcription factor ETS Proto-Oncogene 1 (ETS1) rather than genomic alterations [36]. The prognostic value of EIF4EBP1 extends to other cancers. In hepatocellular carcinoma (HCC), it predicts poor survival [38]. In lung adenocarcinoma (LUAD), compounds like Sauchinone exert anticancer effects by downregulating EIF4EBP1 [39]. Similarly, in renal cell carcinoma, inhibitors like PLX51107 block progression by suppressing EIF4EBP1. These findings support targeting EIF4EBP1 as a viable strategy [40]. Separately, FABP3 has been identified in GBM as an interaction partner for the tumor-homing peptide CooP, mediating the peptide's targeted binding to tumor cells [41]. The MF of FABP3 primarily involves the regulation of lipid metabolism and transport. In invasive glioma cells, FABP3 maintains lysosomal membrane stability by preserving its lipid composition, specifically through the transport of polyunsaturated fatty acids (PUFAs). The loss of FABP3 function leads to lysosomal membrane permeabilization (LMP) and subsequent cell death [42]. KCNQ2 encodes a critical subunit of voltage-gated potassium channels, which are essential for regulating neuronal excitability, primarily by mediating the M-current. Loss-of-function mutations in KCNQ2, often in conjunction with KCNQ3 forming heterotetrameric channels, are a well-established cause of epilepsy and a spectrum of neurodevelopmental disorders [43]. The epithelial cell adhesion molecule (EpCAM), also designated as CD326, is a type I transmembrane glycoprotein predominantly expressed in epithelial tissues and epithelial-derived malignancies. It facilitates homotypic cell-cell adhesion and participates in critical cellular processes, including intracellular signaling, migration, proliferation, and differentiation. Its significant overexpression in a wide spectrum of carcinomas underscores its importance as a diagnostic biomarker and a promising therapeutic target in oncology [44]. In gliomagenesis, EPCAM exerts a significant influence on intercellular connectivity by regulating the stability and turnover of key tight junction proteins, including claudin-7 and claudin-1. This perturbation of junctional integrity compromises cell-cell adhesion and epithelial barrier function, a pathological hallmark that becomes increasingly pronounced in high-grade gliomas [45]. S1PR5, a member of the sphingosine-1-phosphate (S1P) receptor family, may regulate the progression of brain tumors through interactions with other G protein-coupled receptors (GPCRs). Research has identified a specific interaction between S1PR5 and the type 2 cannabinoid receptor (CB2). Furthermore, activation of S1PR5 was found to negatively modulate the CB2 receptor-mediated pro-tumorigenic effects in the human GBM cell line U-87 MG [46]. The findings suggest that S1PR5 may act as a negative regulatory factor for CB2 signaling, potentially exerting a protective function within the pathological process of glioma by counteracting CB2-mediated tumor-promoting effects. KCNQ2 encodes a voltage-gated potassium channel, and its functional loss leads to membrane depolarization, subsequently activating calcium-dependent signaling pathways [e.g., nuclear factor of activated T-cells (NFAT)], which ultimately promote tumor cell proliferation and inhibit differentiation. GRM3 (metabotropic glutamate receptor 3) functions primarily by modulating glutamate signaling pathways to influence tumor biological behavior [47,48]. In the specific context of *IDH*-mutant gliomas, the mechanistic role of GRM3 exhibits a distinct metabolic dependency. Given the high structural homology between D-2-HG and glutamate, D-2-HG acts as a "metabolic mimetic" ligand, directly binding to the extracellular domain of GRM3. Specifically, activation of GRM3—whether by endogenous glutamate or high concentrations of D-2-HG—recruits Gi/o proteins, which subsequently inhibit adenylyl cyclase and significantly suppress intracellular cAMP levels. This sustained low-cAMP environment relieves protein kinase A (PKA)-mediated inhibition of downstream signaling and aberrantly regulates the extracellular signal-regulated kinase (ERK)

pathway, thereby sustaining tumor cell survival and proliferation [48]. Additionally, GRM3 plays a regulatory role in the self-renewal and differentiation processes of glioma stem cells (GSCs). Its expression is positively correlated with key GSC markers, including the transcription factor SRY-box transcription factor 2 (SOX2), suggesting its contribution to the maintenance of stemness in this critical cell population [49].

Based on the current literature review, we have identified that these key genes are implicated in tumorigenesis and cancer progression, with most having been investigated in the context of GBM. Notably, no existing studies have reported direct or indirect interactions between these key genes and D-2-HG. However, through integrated machine learning and molecular docking approaches, our study reveals a close association between these genes and D-2-HG. Given that D-2-HG has been established as a driver in the formation of *IDH*-mutant glioma [50], these findings highlight substantial and valuable research avenues that remain unexplored, underscoring the significance of our current investigation. For instance, EIF4EBP1 acts as a key downstream effector of the mTORC1 complex. Upon phosphorylation by mTORC1, EIF4EBP1 releases the translation initiation factor eIF4E, thereby initiating cap-dependent translation and facilitating the synthesis of pro-oncogenic proteins (e.g., cyclins, growth factors). This process ultimately drives the proliferation, survival, and metabolic reprogramming of glioma cells [51]. By affecting the adenosine monophosphate (AMP)/ATP ratio, D-2-HG could indirectly modulate AMPK activity. This would engage the AMPK-mTORC1-EIF4EBP1 signaling axis, potentially establishing a negative feedback mechanism that limits uncontrolled proliferation and restricts tumor overgrowth [52,53]. This finding corroborates the clinical observation that *IDH*-mutant gliomas typically exhibit a slower growth rate and a more favorable prognosis.

This research encompasses several fundamental limitations. While the sample size is adequate for initial analysis, it could restrict the wider applicability and generalizability of the findings to larger populations. Additionally, while factors such as age, genetic predispositions, and lifestyle choices were somewhat accounted for, there may still be residual influences that could affect the findings. Furthermore, the outcomes predicted through computational methods necessitate further experimental verification to establish their true biological significance and precision, a crucial aim for our forthcoming investigations. Consequently, subsequent investigations ought to focus on augmenting both the magnitude and heterogeneity of the participant group, in addition to utilizing various methodologies, such as *in vitro* and *in vivo* studies, to substantiate and corroborate the significant findings. This approach will enhance the reliability and applicability of the research outcomes. Notwithstanding these limitations, the comprehensive examination of the interconnected molecular pathways between D-2-HG and GBM presented in this research carries considerable implications for public health. Future research should focus on the interactions between these key genes and D-2-HG to explore potential targeted therapeutics for improving the survival prognosis of glioma patients.

5. Conclusion

The present research indicates that D-2-HG could play a role in the development of GBM through the modulation of particular genes. Molecular docking analyses demonstrated notable binding affinity between D-2-HG and its corresponding target proteins. These results establish a basis for additional exploration into the pathways through which D-2-HG may facilitate the onset and advancement of GBM. Future research should focus on elucidating the quantitative relationship between D-2-HG levels and GBM formation and prognosis, as well as exploring potential therapeutic interventions using targeted drugs or natural products for GBM treatment.

Availability of Data and Materials

No supplementary files are uploaded with this submission. The original data supporting this work are available from the corresponding author upon reasonable request.

Author Contributions

JZ and QBW formulated the overall research objectives and purposes of this paper; YFZ is responsible for data retrieval,data processing and analysis in this study; XFY has done important work in molecular docking and image integration; QLL contributed to drafting the manuscript and interpreting the data for the work.; QLL and JZ performed valuable work in revising the paper's content and reviewing the data processing. All authors contributed to critical revision of the manuscript for important intellectual content. All authors read and approved the final manuscript. All authors have participated sufficiently in the work and agreed to be accountable for all aspects of the work.

Ethics Approval and Consent to Participate

This research is to mine the data in the public database, mainly the geo database. This database is open source and does not need additional ethical approval.

Acknowledgment

We would like to express our gratitude to all those who helped us during the writing of this manuscript. Thanks to all the peer reviewers for their opinions and suggestions.

Funding

This research received no external funding.

Conflict of Interest

The authors declare no conflict of interest.

Declaration of AI and AI-Assisted Technologies in the Writing Process

During the preparation of this work, the authors used ChatGPT-3.5 in order to check spelling and grammar. After using this tool, the authors reviewed and edited the content as needed and take full responsibility for the content of the publication.

References

[1] Rahman MA, Yadab MK, Ali MM. Overcoming standard-of-care resistance in glioblastoma using nanoparticle-based drug delivery targeting the autophagy pathway. Biochemical Pharmacology. 2025; 242: 117302. https://doi.org/10.1016/j.bcp.2025.117302.

[2] Haumann R, Videira JC, Kaspers GJL, van Vuurden DG, Hulleman E. Overview of Current Drug Delivery Methods Across the Blood-Brain Barrier for the Treatment of Primary Brain Tumors. CNS Drugs. 2020; 34: 1121–1131. https://doi.org/10.1007/s40263-020-00766-w.

[3] Anwer MS, Abdel-Rasol MA, El-Sayed WM. Emerging therapeutic strategies in glioblastsoma: drug repurposing, mechanisms of resistance, precision medicine, and technological innovations. Clinical and Experimental Medicine. 2025; 25: 117. https://doi.org/10.1007/s10238-025-01631-0.

[4] Amaral M, Cruz N, Rosa A, Nogueira B, Costa D, Santos F, *et al*. An update of advanced nanoplatforms for Glioblastoma Multiforme Management. EXCLI Journal. 2021; 20: 1544. https://doi.org/10.17179/excli2021-4393.

[5] Liu X, Gong Y. Isocitrate dehydrogenase inhibitors in acute myeloid leukemia. Biomarker Research. 2019; 7: 22. https://doi.org/10.1186/s40364-019-0173-z.

[6] He Q, Chen J, Xie Z, Chen Z. Wild-Type Isocitrate Dehydrogenase-Dependent Oxidative Decarboxylation and Reductive Carboxylation in Cancer and Their Clinical Significance. Cancers. 2022; 14: 5779. https://doi.org/10.3390/cancers14235779.

[7] Felsberg J, Wolter M, Seul H, Friedensdorf B, Göppert M, Sabel MC, *et al*. Rapid and sensitive assessment of the IDH1 and IDH2 mutation status in cerebral gliomas based on DNA pyrosequencing. Acta Neuropathologica. 2010; 119: 501–507. https://doi.org/10.1007/s00401-010-0647-4.

[8] Horbinski C, Kofler J, Yeaney G, Camelo-Piragua S, Venneti S, Louis DN, *et al*. Isocitrate dehydrogenase 1 analysis differentiates gangliogliomas from infiltrative gliomas. Brain Pathology (Zurich, Switzerland). 2011; 21: 564–574. https://doi.org/10.1111/j.1750-3639.2011.00480.x.

[9] Wahl DR, Venneti S. 2-Hydoxyglutarate: D/Riving Pathology in gLiomaS. Brain Pathology (Zurich, Switzerland). 2015; 25: 760–768. https://doi.org/10.1111/bpa.12309.

[10] Li T, Cox CD, Ozer BH, Nguyen NT, Nguyen HN, Lai TJ, *et al*. D-2-Hydroxyglutarate Is Necessary and Sufficient for Isocitrate Dehydrogenase 1 Mutant-Induced *MIR148A* Promoter Methylation. Molecular Cancer Research: MCR. 2018; 16: 947–960. https://doi.org/10.1158/1541-7786.MCR-17-0367.

[11] Dang L, Yen K, Attar EC. IDH mutations in cancer and progress toward development of targeted therapeutics. Annals of Oncology: Official Journal of the European Society for Medical Oncology. 2016; 27: 599–608. https://doi.org/10.1093/annonc/mdw013.

[12] Kayabolen A, Yilmaz E, Bagci-Onder T. *IDH* Mutations in Glioma: Double-Edged Sword in Clinical Applications? Biomedicines. 2021; 9: 799. https://doi.org/10.3390/biomedicines9070799.

[13] Yogendran LV, Kareddy A, Abbas SO, Scharf Z, Patrie J, Patel SH, *et al*. Effects of re-challenge with temozolomide in grade 2/3 IDH mutant gliomas at first progression. Journal of Neuro-Oncology. 2025; 175: 1147–1154. https://doi.org/10.1007/s11060-025-05087-w.

[14] Oh S, Cho Y, Chang M, Park S, Kwon H. Metformin Decreases 2-HG Production through the MYC-PHGDH Pathway in Suppressing Breast Cancer Cell Proliferation. Metabolites. 2021; 11: 480. https://doi.org/10.3390/metabo11080480.

[15] Choate KA, Pratt EPS, Jennings MJ, Winn RJ, Mann PB. IDH Mutations in Glioma: Molecular, Cellular, Diagnostic, and Clinical Implications. Biology. 2024; 13: 885. https://doi.org/10.3390/biology13110885.

[16] Leek JT, Johnson WE, Parker HS, Jaffe AE, Storey JD. The sva package for removing batch effects and other unwanted variation in high-throughput experiments. Bioinformatics (Oxford, England). 2012; 28: 882–883. https://doi.org/10.1093/bioinformatics/bts034.

[17] Reynolds M, Chaudhary T, Eshaghzadeh Torbati M, Tudorascu DL, Batmanghelich K, Alzheimer's Disease Neuroimaging Initiative. ComBat Harmonization: Empirical Bayes versus fully Bayes approaches. NeuroImage. Clinical. 2023; 39: 103472. https://doi.org/10.1016/j.nicl.2023.103472.

[18] Yin Y, Chen C, Zhang D, Han Q, Wang Z, Huang Z, *et al*. Construction of predictive model of interstitial fibrosis and tubular atrophy after kidney transplantation with machine learning algorithms. Frontiers in Genetics. 2023; 14: 1276963. https://doi.org/10.3389/fgene.2023.1276963.

[19] Kiefer F, Arnold K, Künzli M, Bordoli L, Schwede T. The SWISS-MODEL Repository and associated resources. Nucleic Acids Research. 2009; 37: D387–D392. https://doi.org/10.1093/nar/gkn750.

[20] Supandi S, Wulandari MS, Samsul E, Azminah A, Purwoko RY, Herman H, *et al*. Dipeptidyl peptidase IV inhibition of phytocompounds from *Artocarpus champeden* (Lour.) Stokes: *In silico* molecular docking study and ADME-Tox prediction approach. Journal of Advanced Pharmaceutical Technology & Research. 2022; 13: 207–215. https://doi.org/10.4103/japtr.japtr_376_22.

[21] Jiang B, Zhang J, Xia J, Zhao W, Wu Y, Shi M, *et al*. IDH1 Mutation Promotes Tumorigenesis by Inhibiting JNK Activation and Apoptosis Induced by Serum Starvation. Cell Reports. 2017; 19: 389–400. https://doi.org/10.1016/j.celrep.2017.03.053.

[22] Yang Z, Jiang B, Wang Y, Ni H, Zhang J, Xia J, *et al*. 2-HG Inhibits Necroptosis by Stimulating DNMT1-Dependent Hypermethylation of the RIP3 Promoter. Cell Reports. 2017; 19: 1846–1857. https://doi.org/10.1016/j.celrep.2017.05.012.

[23] Krell D, Assoku M, Galloway M, Mulholland P, Tomlinson I, Bardella C. Screen for IDH1, IDH2, IDH3, D2HGDH and L2HGDH mutations in glioblastoma. PloS One. 2011; 6: e19868. https://doi.org/10.1371/journal.pone.0019868.

[24] Semukunzi H, Roy D, Li H, Khan GJ, Lyu X, Yuan S, *et al*. IDH mutations associated impact on related cancer epidemiology and subsequent effect toward HIF-1α. Biomedicine & Pharmacotherapy = Biomedecine & Pharmacotherapie. 2017; 89: 805–811. https://doi.org/10.1016/j.biopha.2017.02.083.

[25] Peeters TH, Lenting K, Breukels V, van Lith SAM, van den Heuvel CNAM, Molenaar R, *et al*. *Isocitrate dehydrogenase 1*-mutated cancers are sensitive to the green tea polyphenol epigallocatechin-3-gallate. Cancer & Metabolism. 2019; 7: 4. https://doi.org/10.1186/s40170-019-0198-7.

[26] Cai M, Zhao J, Ding Q, Wei J. Oncometabolite 2-hydroxyglutarate regulates anti-tumor immunity. Heliyon. 2024; 10: e24454. https://doi.org/10.1016/j.heliyon.2024.e24454.

[27] Kim YH, Yoo KC, Cui YH, Uddin N, Lim EJ, Kim MJ, *et al*. Radiation promotes malignant progression of glioma cells through HIF-1alpha stabilization. Cancer Letters. 2014; 354: 132–141.

https://doi.org/10.1016/j.canlet.2014.07.048.
[28] McMahon S, Charbonneau M, Grandmont S, Richard DE, Dubois CM. Transforming growth factor beta1 induces hypoxia-inducible factor-1 stabilization through selective inhibition of PHD2 expression. The Journal of Biological Chemistry. 2006; 281: 24171–24181. https://doi.org/10.1074/jbc.M604507200.
[29] Wang Y, Liu B, Li F, Zhang Y, Gao X, Wang Y, *et al*. The connection between tricarboxylic acid cycle enzyme mutations and pseudohypoxic signaling in pheochromocytoma and paraganglioma. Frontiers in Endocrinology. 2023; 14: 1274239. https://doi.org/10.3389/fendo.2023.1274239.
[30] Chang SL, Seth P, Zhu J, Pendyala G, Bidlack JM, Kumar S. The 27th Scientific Conference of the Society on NeuroImmune Pharmacology: New Delhi, India, March 15-18, 2023. NeuroImmune Pharmacology and Therapeutics. 2023; 2: 187–244. https://doi.org/10.1515/nipt-2023-0006.
[31] Alshiekh Nasany R, de la Fuente MI. Therapies for IDH-Mutant Gliomas. Current Neurology and Neuroscience Reports. 2023; 23: 225–233. https://doi.org/10.1007/s11910-023-01265-3.
[32] Batool SM, Lee H, Muralidharan K, Khan SM, Escobedo AK, Gashi D, *et al*. IDH1-dependent m6A methylation defines transcriptomic heterogeneity in glioma. medRxiv. 2025. https://doi.org/10.1101/2024.09.24.24314089. (preprint)
[33] Solomou G, Finch A, Asghar A, Bardella C. Mutant IDH in Gliomas: Role in Cancer and Treatment Options. Cancers. 2023; 15: 2883. https://doi.org/10.3390/cancers15112883.
[34] Chapman NM, Chi H. Metabolic rewiring and communication in cancer immunity. Cell Chemical Biology. 2024; 31: 862–883. https://doi.org/10.1016/j.chembiol.2024.02.001.
[35] Ma Z, Yang J, Jia W, Li L, Li Y, Hu J, *et al*. Histone lactylation-driven B7-H3 expression promotes tumor immune evasion. Theranostics. 2025; 15: 2338–2359. https://doi.org/10.7150/thno.105947.
[36] Hauffe L, Picard D, Musa J, Remke M, Grünewald TGP, Rotblat B, *et al*. Eukaryotic translation initiation factor 4E binding protein 1 (EIF4EBP1) expression in glioblastoma is driven by ETS1- and MYBL2-dependent transcriptional activation. Cell Death Discovery. 2022; 8: 91. https://doi.org/10.1038/s41420-022-00883-z.
[37] Larriba E, de Juan Romero C, García-Martínez A, Quintanar T, Rodríguez-Lescure Á, Soto JL, *et al*. Identification of new targets for glioblastoma therapy based on a DNA expression microarray. Computers in Biology and Medicine. 2024; 179: 108833. https://doi.org/10.1016/j.compbiomed.2024.108833.
[38] Cha YL, Li PD, Yuan LJ, Zhang MY, Zhang YJ, Rao HL, *et al*. EIF4EBP1 overexpression is associated with poor survival and disease progression in patients with hepatocellular carcinoma. PloS One. 2015; 10: e0117493. https://doi.org/10.1371/journal.pone.0117493.
[39] Li SQ, Feng J, Yang M, Ai XP, He M, Liu F. Sauchinone: a prospective therapeutic agent-mediated EIF4EBP1 down-regulation suppresses proliferation, invasion and migration of lung adenocarcinoma cells. Journal of Natural Medicines. 2020; 74: 777–787. https://doi.org/10.1007/s11418-020-01435-4.
[40] Wan P, Chen Z, Zhong W, Jiang H, Huang Z, Peng D, *et al*. BRDT is a novel regulator of eIF4EBP1 in renal cell carcinoma. Oncology Reports. 2020; 44: 2475–2486. https://doi.org/10.3892/or.2020.7796.
[41] Ayo A, Figueras E, Schachtsiek T, Budak M, Sewald N, Laakkonen P. Tumor-Targeting Peptides: The Functional Screen of Glioblastoma Homing Peptides to the Target Protein FABP3 (MDGI). Cancers. 2020; 12: 1836. https://doi.org/10.3390/cancers12071836.
[42] Le Joncour V, Filppu P, Hyvönen M, Holopainen M, Turunen SP, Sihto H, *et al*. Vulnerability of invasive glioblastoma cells to lysosomal membrane destabilization. EMBO Molecular Medicine. 2019; 11: e9034. https://doi.org/10.15252/emmm.201809034.
[43] Huang Z, Liu B, Xiao T, Wang Y, Lu Y, Hu L, *et al*. Neurodevelopmental Outcomes Prediction in Newborns with Seizures Caused by KCNQ2 Gene Defects. Neonatology. 2024; 121: 178–186. https://doi.org/10.1159/000534605.
[44] Patriarca C, Macchi RM, Marschner AK, Mellstedt H. Epithelial cell adhesion molecule expression (CD326) in cancer: a short review. Cancer Treatment Reviews. 2012; 38: 68–75. https://doi.org/10.1016/j.ctrv.2011.04.002.
[45] Wu CJ, Mannan P, Lu M, Udey MC. Epithelial cell adhesion molecule (EpCAM) regulates claudin dynamics and tight junctions. The Journal of Biological Chemistry. 2013; 288: 12253–12268. https://doi.org/10.1074/jbc.M113.457499.
[46] Kim Y, Ghil S. Negative regulation of cannabinoid receptor 2 induced tumorigenic effect by sphingosine 1 phosphate receptor 5 activation. Oncology Reports. 2025; 53: 41. https://doi.org/10.3892/or.2025.8874.
[47] Maier JP, Ravi VM, Kueckelhaus J, Behringer SP, Garrelfs N, Will P, *et al*. Inhibition of metabotropic glutamate receptor III facilitates sensitization to alkylating chemotherapeutics in glioblastoma. Cell Death & Disease. 2021; 12: 723. https://doi.org/10.1038/s41419-021-03937-9.
[48] Wirsching HG, Silginer M, Ventura E, Macnair W, Burghardt I, Claassen M, *et al*. Negative allosteric modulators of metabotropic glutamate receptor 3 target the stem-like phenotype of glioblastoma. Molecular Therapy Oncolytics. 2021; 20: 166–174. https://doi.org/10.1016/j.omto.2020.12.009.
[49] Sareddy GR, Pratap UP, Venkata PP, Zhou M, Alejo S, Viswanadhapalli S, *et al*. Activation of estrogen receptor beta signaling reduces stemness of glioma stem cells. Stem Cells (Dayton, Ohio). 2021; 39: 536–550. https://doi.org/10.1002/stem.3337.
[50] Riviere-Cazaux C, Lacey JM, Carlstrom LP, Laxen WJ, Munoz-Casabella A, Hoplin MD, *et al*. Cerebrospinal fluid 2-hydroxyglutarate as a monitoring biomarker for IDH-mutant gliomas. Neuro-oncology Advances. 2023; 5: vdad061. https://doi.org/10.1093/noajnl/vdad061.
[51] Ryskalin L, Lazzeri G, Flaibani M, Biagioni F, Gambardella S, Frati A, *et al*. mTOR-Dependent Cell Proliferation in the Brain. BioMed Research International. 2017; 2017: 7082696. https://doi.org/10.1155/2017/7082696.
[52] Gwinn DM, Shackelford DB, Egan DF, Mihaylova MM, Mery A, Vasquez DS, *et al*. AMPK phosphorylation of raptor mediates a metabolic checkpoint. Molecular Cell. 2008; 30: 214–226. https://doi.org/10.1016/j.molcel.2008.03.003.
[53] Burgos SA, Kim JJM, Dai M, Cant JP. Energy depletion of bovine mammary epithelial cells activates AMPK and suppresses protein synthesis through inhibition of mTORC1 signaling. Hormone and Metabolic Research = Hormon- Und Stoffwechselforschung = Hormones et Metabolisme. 2013; 45: 183–189. https://doi.org/10.1055/s-0032-1323742.